Analysis of Viscous Free Surface Flow around a Ship by a Level-set Method

Il-Ryong Park[1] and Ho-Hwan Chun[1]

[1]Department of Naval Architecture & Ocean Engineering, Pusan National University, 30, Changjeon-Dong, Kumjeong-Ku, Pusan 609-735, Korea; E-mail: chunahh@hyowon.pusan.ac.kr

Abstract

In the present numerical simulation of viscous free surface flow around a ship, two-fluids incompressible Reynolds- averaged Navier-Stokes equations with the standard $k-\varepsilon$ turbulence model are discretized on a regular grid by using a finite volume method. A local level-set method is introduced for capturing the free surface movement and the influence of the viscous layer and dynamic boundary condition of the free surface are implicitly considered. Partial differential equations in the level-set method are discretized with second order ENO scheme and explicit Euler scheme in the space and time integration, respectively. The computational results for the Series-60 model with $C_B=0.6$ show a good agreement with the experimental data, but more validation studies for commercial complicated hull forms are necessary.

Keywords: local level-set method, viscous free surface flow, RANS equations, finite volume method

1 Introduction

In the field of ship hydrodynamics, it is of prime importance to develop an accurate and efficient numerical scheme for the calculation of viscous free surface flow around a hull by using computational fluid dynamics(CFD). It takes much effort and time to generate grid topology and also long computation time for viscous free surface flow analysis for ships while the potential flow analysis is relatively easy in terms of computational time and numerical handling. However, the rapid growth of the computer technology and the development of new numerical techniques enable speedy simulations of these viscous free surface problems to become possible. In recent papers for the viscous ship wave problems, there are many outstanding computational results(Farmer et al 1994, Hino 1994, Bet et al 1998, Tahara and Stern 1996, Lee 1997, Kim 2000, Kim and Kim 2001). These numerical results show good agreements with experimental results on wave patterns and hydrodynamic forces, but it is still necessary to improve the solutions of viscous dominant flows, stern flow and bow breaking wave, etc. As of recent days, boundary element method has been efficiently used to solve the nonlinear behaviors of wave breaking or more complicated free surface phenomena. With the development of computational fluid dynamics, various complex interacting interface and multi-phase problems with viscous effect which are difficult for the boundary element methods to treat have been analyzed by viscous flow solvers with various free surface treatments.

For the free surface treatment, two main approaches, front tracking & front capturing methods, have been used. In front capturing methods, the level-set scheme which is taken as the present numerical method for capturing the free surface has been only recently used in ship hydrodynamic problems(Vogt 1998, Bet et al 1998, Park and Chun 1999(a), Park and Chun 1999(b), Hochbaum and Schumann 1999, Hino 2000, Hochbaum and Vogt 2000, Park 2000). The level-set method is a numerical technique which can follow the evolution of interfaces. These interfaces can develop sharp corners, break apart, and merge together. The level-set method has a wide range of applications such as fluid mechanics, combustion, manufacturing of computer chips, computer animation, image processing, structure of snowflakes, and the shape of soap bubbles. Especially for many complex free surface problems(e.g. breaking wave, spray phenomena, sloshing in a liquid tank, slamming problem, water-exit problem and bubble problem) in the naval hydrodynamics, this method is a provocative approach that could be used as a robust numerical scheme. The level-set method doesn't need the complex bookkeeping scheme in the computational procedure. It is rather easier to extend the level-set method to three-dimensional problems. On the other hand, there are some drawbacks compared with the front tracking methods. High order accuracy and area or volume conservation can be lost more or less around the free surface and a special treatment must be introduced for maintaining the uniform thickness around the interface. Although these drawbacks exist in the level-set method, the drawback of the front tracking method can be avoided by using the level-set method and it is certified from the systematic application to two- and three-dimensional complex hydrodynamic problems with the free surface conducted by Vogt(1998), Park and Chun(1999(a), 1999(b)) and Park(2000).

In the present paper, a local level-set method is introduced for capturing the free surface movement and the dynamic boundary condition of the free surface is implicitly considered. Two-fluids Reynolds-averaged Navier-Stokes(RANS) equations are solved on a regular grid by using a finite volume method. The present discretizations of the governing equations are of second order in space integration. The standard $k - \varepsilon$ turbulence model is employed for the turbulence closure. The numerical results for the Series-60 model with C_B=0.6 are compared with experimental results taken from Toda et al(1991). The present study intends to investigate the numerical characteristics and applicability of the local level-set scheme in ship wave problems.

2 Mathematical formulation

2.1 Governing equations

In the three-dimension problem, the general integral level-set form of the time-averaged conservation equations of mass, two-fluids incompressible Navier-Stokes equations and turbulent kinetic energy dissipation rate can be written as

$$\iiint_\Omega \frac{\partial}{\partial t}(\rho(\phi)q)d\Omega + \iint_S (\rho(\phi)\mathbf{u}q - \Gamma_q(\phi)\nabla q) \cdot d\mathbf{S} = \iiint_\Omega S_q d\Omega \qquad (1)$$

where $\mathbf{u} = (u_1, u_2, u_3)$ is the velocity vector of fluid, q is any conservative quantity, Γ_q is the associated diffusive coefficient, S_q is the volumetric source term of q and ρ is the fluid density. ϕ is a level-set function and the details of the level-set method will be described in the next chapter.

This integral level-set form equation contains implicitly the air-water boundary condition, namely, the dynamic free surface boundary conditions. Equation (1) can be written in the vec-

tor form as

$$\iiint_\Omega \frac{\partial \mathbf{U}}{\partial t} d\Omega + \iint_S (\mathbf{F_{conv}} - \mathbf{F_{diff}}) \cdot d\mathbf{S} = \iiint_\Omega \mathbf{B} d\Omega \qquad (2)$$

where vectors $\mathbf{U}$, $\mathbf{F_{conv}} - \mathbf{F_{diff}}$ and $\mathbf{B}$ are defined as

$$\mathbf{U} = \begin{bmatrix} 0 \\ \rho(\phi)u_1 \\ \rho(\phi)u_2 \\ \rho(\phi)u_3 \\ \rho(\phi)k \\ \rho(\phi)\varepsilon \end{bmatrix}, \mathbf{B} = \begin{bmatrix} 0 \\ \rho(\phi)g_1 - p\vec{i} \\ \rho(\phi)g_2 - p\vec{j} \\ \rho(\phi)g_3 - p\vec{k} \\ G_k - \rho(\phi)\varepsilon \\ (C_1 G_k - C_2\rho(\phi)\varepsilon)\frac{\varepsilon}{k} \end{bmatrix}, \mathbf{F_{conv}} - \mathbf{F_{diff}} = \begin{bmatrix} \rho(\phi)u - 0 \\ \rho(\phi)uu_1 - \mu_{eff}(\phi)(\nabla u_1) \\ \rho(\phi)uu_2 - \mu_{eff}(\phi)(\nabla u_2) \\ \rho(\phi)uu_3 - \mu_{eff}(\phi)(\nabla u_3) \\ \rho(\phi)uk - \frac{\mu_{eff}(\phi)}{\sigma_k}(\nabla k) \\ \rho(\phi)u\varepsilon - \frac{\mu_{eff}(\phi)}{\sigma_\varepsilon}(\nabla \varepsilon) \end{bmatrix}$$

$$\qquad (3)$$

where p is the pressure, k is the turbulent kinetic energy, ε is the turbulent dissipation rate, $\mu_{eff} = \mu + \mu_t$, μ is the viscosity of the fluid, μ_t is the turbulent eddy viscosity and G_k is the rate of production of turbulence kinetic energy defined as

$$G_k = \mu_t\{2(\frac{\partial u_1^2}{\partial x} + \frac{\partial u_2^2}{\partial y} + \frac{\partial u_3^2}{\partial z}) + (\frac{\partial u_2}{\partial x} + \frac{\partial u_1}{\partial y})^2 + (\frac{\partial u_3}{\partial y} + \frac{\partial u_2}{\partial x})^2 + (\frac{\partial u_1}{\partial z} + \frac{\partial u_3}{\partial x})^2\} \qquad (4)$$

The constants of the standard $k - \varepsilon$ turbulence model are defined in Table 1.

Table 1: Constants of the standard $k - \varepsilon$ turbulence model

C_μ	C_1	C_2	σ_k	σ_ε	χ
0.09	1.44	1.92	1.0	$\frac{\chi^2}{(C_2-C_1)\sqrt{C_\mu}}$	0.41

2.2 Level-set formulation

As seen in Figure 1, the immiscible and incompressible two-phase fluids are described by their densities (ρ_1,ρ_2) and viscosities (μ_1,μ_2), where these physical properties are constant in each subdomain. In the fluid domain Ω, the interface Γ represents a boundary of two fluids and through this boundary the physical properties are discontinuous. The interface moves with the flow according to the velocity field, and the deformation and movement of the interface influence the velocity field. Moving interface problems can be formulated as level-set functions on a fixed domain, where the interface is zero-level-set:

$$\Gamma = \{\mathbf{x} \in R^3 : \phi(\mathbf{x}, t) = 0\} \qquad (5)$$

There are many functions for describing the zero-level-set, Γ. The signed distance level-set function is more stable and suitable for describing the interface. At one side of the interface the level-set function can be defined as the following conditions:

$$\Omega_1 = \{\mathbf{x} \in R^3 : \phi(\mathbf{x}, t) > 0\} \qquad (6)$$

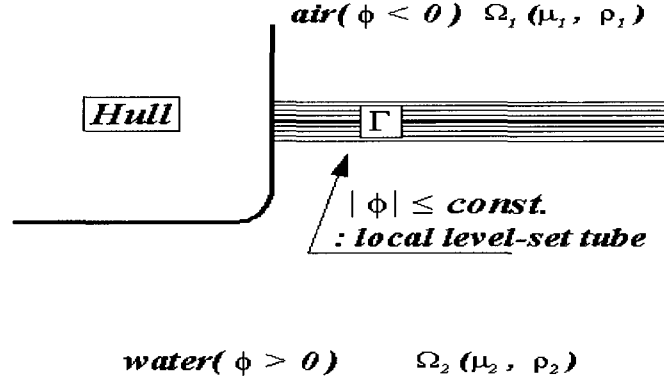$$\Omega_2 = \{\mathbf{x} \in R^3 : \phi(\mathbf{x}, t) < 0\} \qquad (7)$$

Figure 1: Definition sketch of the flow domain

These formulas can be calculated everywhere that $\phi(\mathbf{x}, t)$ is known. The movement of the interface can be described by solving a Hamilton-Jacobi type equation.

$$\frac{\partial \phi}{\partial t} + \mathbf{u} \cdot \nabla \phi = 0 \tag{8}$$

This approach allows merging, breaking and other topological changes to be handled automatically. In the present work, second order ENO scheme(Harten et al 1987) is used for spatial derivative in (8) and explicit Euler scheme is used for time integration.

2.2.1 Thickness of the interface

By the definition of this level-set function, the density and viscosity coefficients can be defined as follows:

$$\rho(\phi) = \rho_1 + (\rho_2 - \rho_1)H(\phi) \tag{9}$$

$$\mu(\phi) = \mu_1 + (\mu_2 - \mu_1)H(\phi) \tag{10}$$

where $H(\phi > 0) = 1$, $H(\phi < 0) = 0$ and $H(\phi = 0) = 1/2$.

Since density and viscosity change sharply across the interface, it is necessary to give the interface a fixed thickness that is proportional to the grid size. This allows to replace $\rho(\phi)$ and $\mu(\phi)$ by smoothed functions, $\rho_\omega(\phi)$, $\mu_\omega(\phi)$, which are given by

$$\rho_\omega(\phi) = \rho_1 + (\rho_2 - \rho_1)H_\omega(\phi) \tag{11}$$

$$\mu_\omega(\phi) = \mu_1 + (\mu_2 - \mu_1)H_\omega(\phi) \tag{12}$$

with

$$H_\omega(\phi) = \begin{cases} 0 & \text{if} \quad \phi < -\omega \\ \frac{1}{2}(1 + \frac{\phi}{\omega} + \frac{1}{\pi}sin(\pi\frac{\phi}{\omega})) & \text{if} \quad |\phi| \leq \omega \\ 1 & \text{if} \quad \phi > \omega \end{cases} \tag{13}$$

where ω is the thickness of the interface and this value can be defined by $\omega = \alpha\Delta h$, where α is constant which is usually taken as 2~4 and Δh is the grid size.

2.2.2 Reinitialization procedure

Even though the evolution equation (8) is computed accurately, the initial signed distance property of the level-set function ϕ_0 could be destroyed due to flat and/or steep regions at the interface. As calculation goes on, the magnitude of the level-set gradient $|\nabla\phi|$ fails to maintain to have unity. This makes computation, level-set contour plotting and conservative properties highly inaccurate. In order to prevent these inaccuracies, it is necessary to reconstruct the level-set function at each computational time. This process is called reinitialization. In the present work, the following partial differential equation is introduced for the reinitialization process(Sussman et al 1997).

$$\frac{\partial d}{\partial \tau} + sign(d_0)(|\nabla d| - 1) = 0$$

$$d(\mathbf{x}, 0) = d_0(\mathbf{x}) = \phi(\mathbf{x}, \tau) \tag{14}$$

where τ is a dummy time which is only used for the reinitialization procedure, $sign(d_0) = 1$ if $d_0 > 0$, $sign(d_0) = -1$ if $d_0 < 0$, and $sign(0) = 0$.

The idea of this equation is that a steady-state solution will be a signed distance function that has $|\nabla d| = 1$ near the interface with the same zero-level-set as the initial function $d_0(\mathbf{x})$. The value $d(\mathbf{x}, \tau)$ propagates with speed ± 1 along the characteristics that are normal to the interface and converges quickly in a neighborhood of the interface for small time τ. Second order ENO scheme is used for spatial derivative $|\nabla d|$ in (14) and explicit Euler scheme is used for time integration.

The width of the neighborhood around the interface can be defined $\alpha\Delta h$, where $\alpha > 0$, and it is sufficient to solve (14) up to time $\alpha\Delta h$. Since the characteristics propagate away from the interface with speed of unity, the appropriate time step according to the CFL(Courant Friedriches Lewy) condition is $\Delta\tau = \Delta h/2 \sim \Delta h/5$.

2.2.3 Local level-set method

According to the property of locality of the level-set method, it is sufficient to calculate the level-set function only in a small narrow band around its zero-level-set for the reinitialization procedure. In the case of two-dimensional computation, let $N \times N$ be the number of grid point and then computational expense reduces from $O(N^2)$ to $O(N)$ by the help of the locality property of the level-set method(Peng et al 1999). In the present paper, a PDE-based local level-set method developed by Peng et al(1999) is used.

3 Numerical procedure

In the discretization process, all unknown values and physical properties are computed and stored at the center of the control volume. Interpolation and differentiation are necessary to evaluate the convective and diffusive fluxes at the cell-face center and each flux can be approximated with the midpoint rule as follows:

$$\text{Mass \quad flux}: \quad \dot{m}_e = \iint_{S_e} \rho(\phi)\mathbf{u} \cdot d\mathbf{s} \approx [\rho(\phi)\mathbf{u} \cdot \mathbf{n}]_e S_e \tag{15}$$

$$\text{Convective \quad flux}: \quad \dot{m}_e q_e \tag{16}$$

$$\text{Diffusive \quad flux}: \quad [\Gamma_q(\phi)\nabla q \cdot \mathbf{n}]_e S_e \tag{17}$$

Figure 2: Non-orthogonal grid element

The hybrid scheme is used to approximate convective fluxes. For the approximations of the diffusive fluxes, the gradient vector at the cell face can be calculated from the gradients at the cell centers approximated by using midpoint rule based on the Gauss theorem:

$$(\nabla q)_{\mathbf{P}} \approx \frac{\iiint_{\Omega}(\nabla q)d\Omega}{\Delta\Omega} = \frac{\iint_{S} \vec{q^{i}} \cdot d\mathbf{S}}{\Delta\Omega} \approx \frac{\sum_{c} q_{c}S_{c}^{i}}{\Delta\Omega} \quad (\mathbf{c} = \mathbf{e, w, n, s}, ...) \tag{18}$$

As seen in Figure 2, when the grid is non-orthogonal, the line connecting points **P** and **E** does not pass through the cell face center e. For the case of a non-orthogonal grid system, Muzafer-ija(1994) suggested an effective scheme, 'differed correction method', to prevent the oscillatory solutions:

$$(\nabla q)_{e} \cdot \mathbf{n}_{e} = (\frac{\partial q}{\partial n})_{e} \approx \frac{q_{\mathbf{E}} - q_{\mathbf{P}}}{L_{\mathbf{P,E}}} + [(\overline{\frac{\partial q}{\partial n}})_{e} - (\overline{\frac{\partial q}{\partial \xi}})_{e'}]^{old} \tag{19}$$

Equation (19) can be rewritten by as follows:

$$\begin{aligned}(\frac{\partial q}{\partial n})_{e} &\approx \frac{q_{\mathbf{E}} - q_{\mathbf{P}}}{L_{\mathbf{P,E}}} + [\frac{q_{\mathbf{E'}} - q_{\mathbf{P'}}}{L_{\mathbf{P',E'}}} - \overline{(\nabla q)_{e'}}\vec{gi_{\xi}}]^{old} \\ &= \frac{q_{\mathbf{E}} - q_{\mathbf{P}}}{L_{\mathbf{P,E}}} + [\frac{q_{\mathbf{E}} - q_{\mathbf{P}}}{L_{\mathbf{P',E'}}} + \frac{(\nabla q)_{\mathbf{E}} \cdot (\vec{r_{\mathbf{E'}}} - \vec{r_{\mathbf{E}}}) - (\nabla q)_{\mathbf{P}} \cdot (\vec{r_{\mathbf{P'}}} - \vec{r_{\mathbf{P}}})}{L_{\mathbf{P',E'}}} \\ &- \{\lambda_{e'}(\nabla q)_{\mathbf{E}} + (1 - \lambda_{e'})(\nabla q)_{\mathbf{P}}\} \cdot \vec{i_{\xi}}]^{old}\end{aligned} \tag{20}$$

where $\vec{i_{\xi}}$: the unit vector in the ξ-direction and over bar denotes interpolation from neighbor nodal values.

$$q_{\mathbf{P'}} = q_{\mathbf{P}} + (\nabla q)_{\mathbf{P}} \cdot (\vec{r_{\mathbf{P'}}} - \vec{r_{\mathbf{P}}}) \tag{21}$$

$$\lambda_{e'} = \frac{|\mathbf{r_{e}} - \mathbf{r_{P'}}|}{|\mathbf{r_{E'}} - \mathbf{r_{P'}}|} \tag{22}$$

$$\vec{r_{\mathbf{P'}}} = \vec{r_{\mathbf{e}}} - [\frac{(\vec{r_{\mathbf{e}}} - \vec{r_{\mathbf{P}}}) \cdot \vec{n_{\mathbf{P}}}}{\vec{n_{\mathbf{e}}} \cdot \vec{n_{\mathbf{P}}}}]\vec{n_{\mathbf{e}}} \tag{23}$$

$$\vec{r_{\mathbf{P'}}} = \vec{r_{\mathbf{e}}} - [(\vec{r_{\mathbf{e}}} - \vec{r_{\mathbf{P}}}) \cdot \vec{n_{\mathbf{P}}}]\vec{n_{\mathbf{e}}}, \quad \text{if} \quad \vec{n_{\mathbf{e}}} \approx \vec{n_{\mathbf{P}}} \tag{24}$$

42

The explicit term at the cell face is used to consider the influence of the cross derivative. On a non-orthogonal grid system, values of fluid properties at the cell face center can be approximated as

$$
\begin{aligned}
q_e &= q_{E'}\lambda_e + q_{P'}(1 - \lambda_e) \\
&= q_E\lambda_e + q_P(1 - \lambda_e) + (\nabla q)_E \cdot (\overrightarrow{r_{E'}} - \overrightarrow{r_E})\lambda_e + (\nabla q)_P \cdot (\overrightarrow{r_{P'}} - \overrightarrow{r_P})(1 - \lambda_e)
\end{aligned} \tag{25}
$$

The implicit Euler scheme is used for the time integration as follows:

$$
\int_{t_n}^{t_{n+1}} \{\frac{\partial q}{\partial t} + f(q(t), t)\}dt = 0 \rightarrow q^{n+1} = q^n + \Delta t[f(t_{n+1}, q^{n+1})] \tag{26}
$$

The discretized linear algebraic equation system is solved by using a conjugate gradient method. SIMPLEC(Semi-Implicit Method for Pressure-Linked Equation Consistent)-algorithm is used for pressure-velocity coupling on cell-centered grids(van Doormal and Rathby 1984).

4   Results and discussions

As computational example, the steady flow around the Series-60 model(C_B =0.6) with the free surface is simulated. The x-axis and y-axis are taken to be positive in the downstream direction and to the starboard side of the hull, respectively. The z-axis is positive upwards. Figure 3 shows a partial view of H-H single structured grid around a Series-60 model and the z-plane grids at the top plane of the computational domain. The grid resolution is taken higher around the free surface and near the hull surface. The computational domain in x, y and z-direction are -1.5$\leq$ x/L $\leq$2.0, 0$\leq$ y/L $\leq$1.0 and -1.0$\leq$ z/L $\leq$0.15, where L(=2.0) is ship length. The length of the extended computational domain above the waterline is 0.15L. In order to check the grid dependency of the present numerical solutions, three computational grids with 98×36×48, 120×44×50, 140×66×50 CV_S are employed. Computations are done at a Froude number $F_n(=U_0/\sqrt{gL})$=0.316 and Reynolds number $R_n(=U_0L\rho/\mu)$=4×10^6, where U_0 is ship speed.
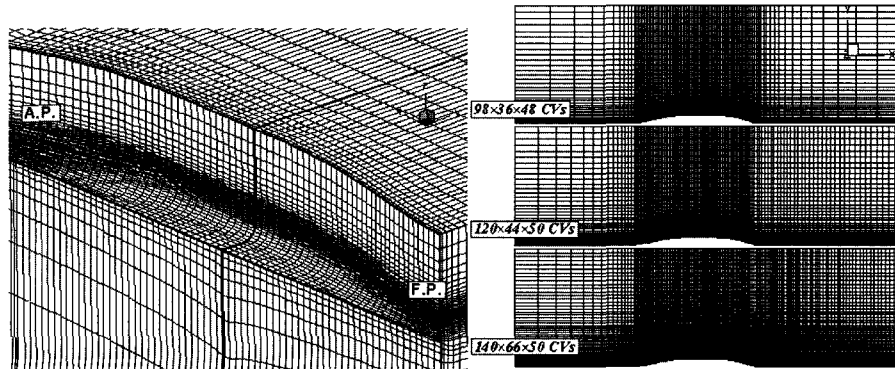
Figure 3: Partial view of a H-H type single structured grid around a Series-60 model and z-plane grids at the top of the computational domain

4.1 Boundary conditions

No slip condition is used at the hull boundary and symmetry boundary condition is applied at the center plane, side plane and bottom of the flow domain. The natural Neumann boundary condition for the pressure is implied at all boundaries of the flow domain. Wall function technique(Launder and Spalding 1974) is used for the turbulence flow boundary conditions near the wall surface. The inflow boundary conditions for the velocity and turbulence equations are following conditions:

$$u_1 = U_0, \quad u_2 = 0, \quad u_3 = 0$$

$$k = k_{in}, \quad \varepsilon = \varepsilon_{in} \tag{27}$$

where the constants K_{in} and ε_{in} have some small positive value.

Computations are started at the full speed U_0 without any flow acceleration. At the outflow, the extrapolation boundary conditions for the velocities and free surface height are used and any quantity is not prescribed and no wave damping area exits.

The dynamic free surface boundary condition is indirectly satisfied with the solutions of the level-set form governing equations and the correct kinematic condition is obtained from the solution of (8).

4.2 Computational results

Figure 4 shows the convergence history of the residuals of the pressure correction and turbulence kinetic energy equation for the three grids, where the time segments for coarse and medium grids have the same size of Δt=0.005 while Δt=0.0025 is used for the fine grid. It can be seen that for all cases, the residuals decrease to about 1×10^{-6} after nondimensional time $t'(=tU_0/L)$=5.

In Figure 5, the time histories of the pressure and friction resistance coefficient for the three grids are plotted as function of the nondimensional time. It can be seen that in all cases, the pressure and friction resistance coefficients converge, showing that the friction resistance converges faster than the pressure resistance.

Table 2 shows a comparison of computed resistance coefficients and experimental results. In the experiment by Toda et al(1991), only the total resistance was measured and the friction resistance coefficient is calculated by the ITTC 1957 correlation line. Then, the sum of the pressure drag and wave resistance coefficient is obtained by subtracting the friction resistance coefficient
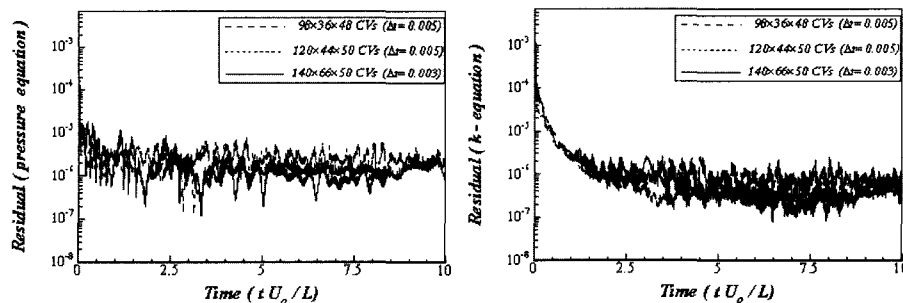
Figure 4: Convergence history of residuals of pressure correction and turbulence kinetic energy equations for three different grids at F_n=0.316, R_n=4.0×10⁶
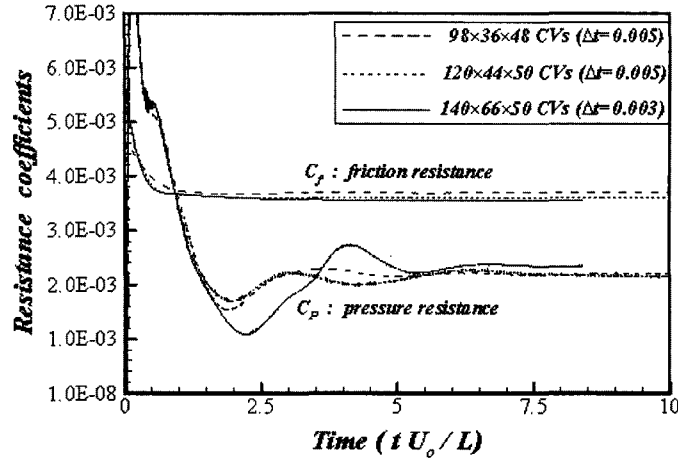
Figure 5: Convergence history of the pressure and friction resistance coefficients for three different grids at F_n=0.316, R_n=4.0×10^6

from the measured total resistance coefficient. Therefore, the comparison of the computed and measured total resistance coefficient is more reliable. It can be seen from the Table 2 that the present computational results for the three grids show good correlation with the experiment. The differences in the results computed by three grids are very small and this is due to the fact that the coarse grid(98×36×48) among the three grids is relatively fine enough for the flow analysis of a simple hull form such as Series 60. In addition, despite the use of H-H type single structured grid, the good agreement between the computation and experiment is also due to the simple geometry.

Figure 6 shows the pressure distributions on the hull of Series-60 model and on the center plane for the fine grid case. The pressure distribution includes the effect of the free surface and shows reasonably converged solution that is similar to other published results(Hino 1994, Tahara and Stern 1996). The pressure lines are concentrated at the free surface boundary and it seems to make one thick line. These pressure lines concentrated around the free surface indicate the use of the interface thickness through which the density and viscosity of the air and water vary according to (13). So this region decreases or increases according to the value of the interface thickness.

Figure 7 shows local level-set function tubes, well converged, along the hull surface and at the fore and after hull, where the thick black line is zero level-set and the free surface plane. When a level-set method is used for capturing the free surface, the reinitialization procedure, described in section 2.2.2, is important to keep the value of the level-set gradient unity around the free surface,

Table 2: Comparison of resistance coefficients

|	C_P	C_f	C_T
Experiment	2.437×10^{-3}	3.522×10^{-3}	5.959×10^{-3}
coarse	0.156×10^{-3}	3.695×10^{-3}	5.851×10^{-3}
medium	2.223×10^{-3}	3.603×10^{-3}	5.826×10^{-3}
fine	2.336×10^{-3}	3.543×10^{-3}	5.879×10^{-3}
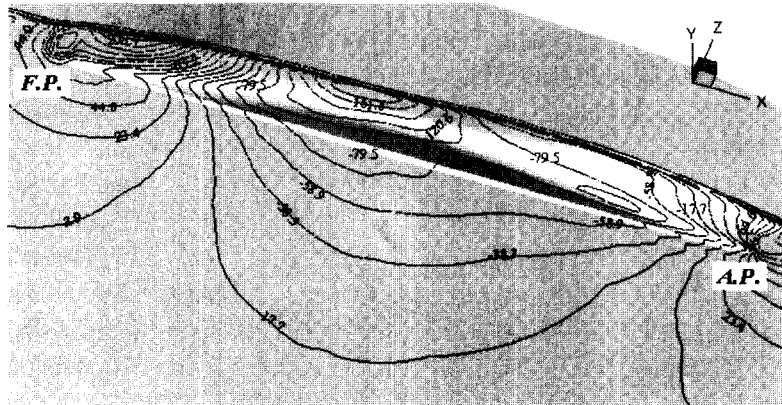
Figure 6: Computed pressure distribution around the hull surface and center plane at F_n=0.316, R_n=4.0×10⁶(fine grid used)

at least in the interface thickness defined in the computations. If this procedure may not be kept, the level-set distributions cannot make a nice and neat uniform appearance and it becomes difficult to proceed to the next time step in computation process.

Figure 8 shows the computed wave patterns for the three grids and it can be seen that the fine grid produces a broader and clear wave pattern than those by other two grids. In Figure 9, the computed wave elevations along the hull surface, $F.P./L$ at -0.5 and $A.P./L$ at 0.5 in x-axis, for the three grids are compared with the measured result taken by Toda et al(1991). As the grid becomes finer, the computed result becomes closer to the experiment. It is known from other published results for the free surface viscous flow analysis around hulls that the computed wave profiles along the hull surfaces show good correlation with the experimental results, better correlation than that by potential flow analysis(Kim 2000). However, the divergent wave patterns in downstream calculated by the most viscous flow solvers are not as clear as the potential flow solutions are. This may be due to the fact that viscous flow solvers have more or less numerical diffusion errors through the free surface while proceeding computations. This kind of phenomena can be also seen in the present computation.
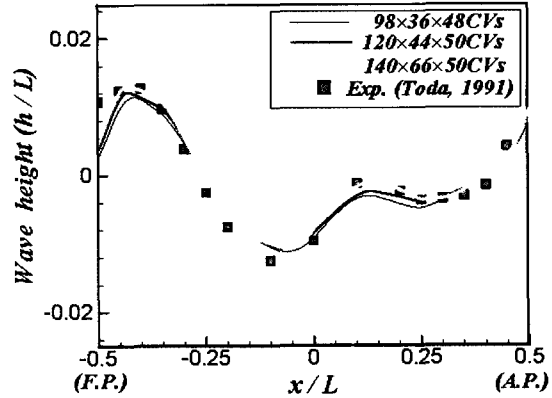
Figure 10 show the comparison between the computed, by the fine grid, and measured lon-
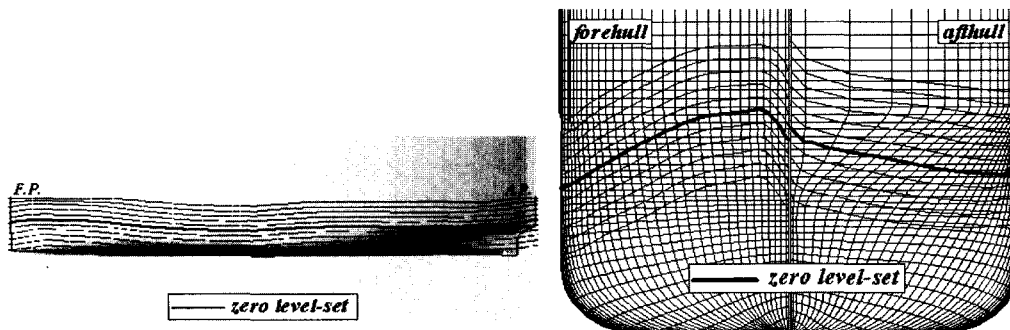
Figure 7: Computed level-set value distributions on the hull surface of the Series-60 model
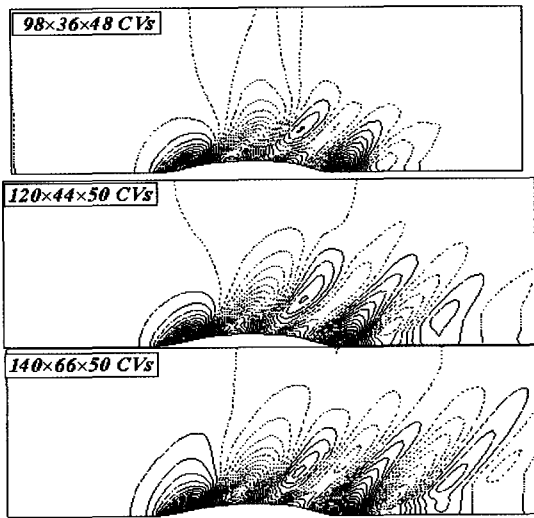
**Figure 8:** Computed wave patterns for three grids around the Series-60 model at F_n=0.316, R_n=4.0×10⁶

Figure 9: Comparison of wave profiles along the hull surface for three grids around the Series-60 model at F_n=0.316, R_n=4.0×10⁶

gitudinal wave cuts at four transverse positions. The fore and after perpendicular($F.P./L$ and $A.P./L$) of the model are located at x=-0.5 and 0.5, respectively, in the axis of the figure. In the near two positions to the hull, y/L=0.0775 and 0.1083, the numerical results show good agreement with the experiment. However, as y/L increases, the agreement is not so good. The present numerical method, the level-set method, is one of the free surface capturing methods and in general, it requires high grid resolution compared with surface tracking methods to have good wave pattern that is close to the experiment. In this view, a finer grid seems to be necessary for the present numerical scheme to enhance its accuracy in predicting the wave pattern. It is worthwhile mentioning that in general, the front tracking method produces better wave patterns, closer to the experiment, than the front capturing method. In addition, when a front capturing method like the present level-set method is used to solve the wave problems, it is important to keep an orthogonal and uniform appearance grid shape around the free surface region, requiring a lot of endeavors and a skillful grid generation.
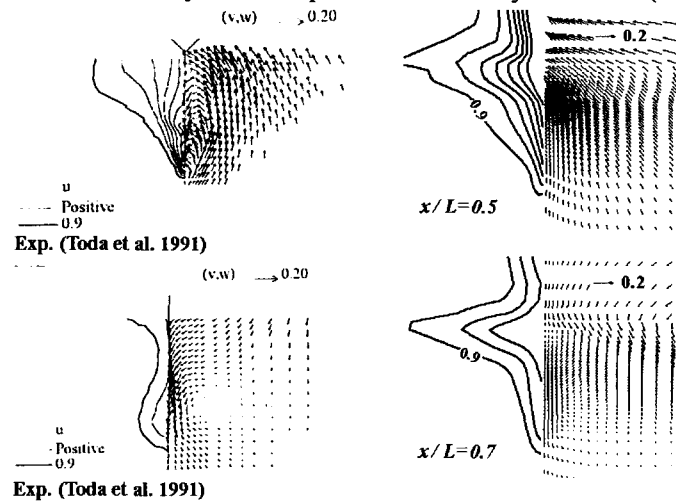
In Figure 11, the computed axial velocity distributions at x/L=0.5 and x/L=0.7 stations are plotted together with the experiments. The whole features are similar to the experimental results, but some discrepancy between the computational and experimental results can be seen. In the numerical results by Hino(1994) and Kim et al(1999), it is mentioned that more appropriate turbulence models should be used for a good prediction of the wake distribution rear the ship hull and if sufficient grid points are adapted around the stern region, the grid dependence in the numerical wake prediction is not so significant.

5 Conclusions

The local level-set approach to solve viscous free surface flows around a hull has been developed. The level-set method is one of Eulerian methods and this method may be suitable for large de-
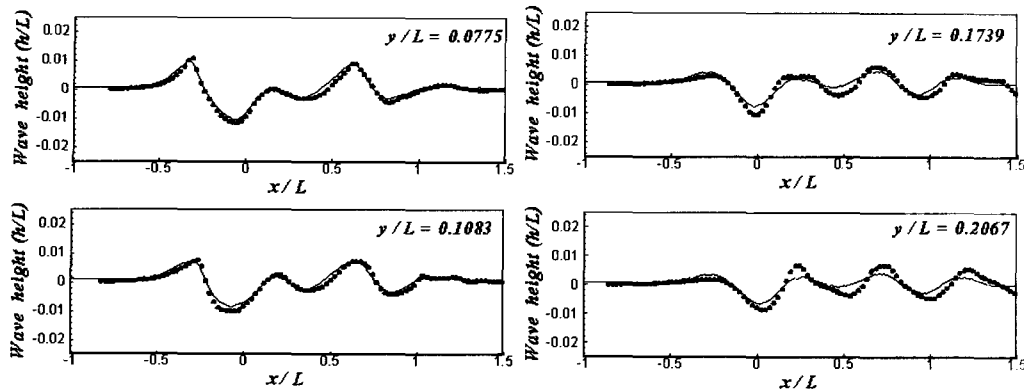
Figure 10: Comparison of longitudinal cut wave profiles at y/L=0.0775, 0.1083, 0.1739 and 0.2067 around the Series-60 model at F_n=0.316, R_n=4.0×10⁶, fine grid used(Solid line: calculation, Black circle symbol: Experiment Taken by Toda et al(1991))

Figure 11: Comparison of axial velocity contours and transverse velocity distributions at x/L=0.5 & 0.7 at F_n=0.316, R_n=4.0×10⁶

formable free surface problems, but the present computed result for Series-60 model demonstrates that the level-set method can give reasonable accurate solutions for ship hydrodynamic problems. More studies are still necessary to validate present work such as real hull forms.

Acknoledgement

References

BET, F., HANEL, D. AND SHARAMA, S.   1998   Numerical Simulation of Ship Flow by a

Method of Artificial Compressibility. Proceedings of the Twenty-Second Symposium on Naval Hydrodynamics, Washington, pp. 173-182

FARMER, J., MARTINELLI, L. AND JAMESON, A. 1994 Multi-grid Solutions of the Euler and Navier-Stokes Equations for a Series-60 C_B=0.6 Ship Hull. Proceedings of CFD Workshop Tokyo

HARTEN, A., ENGQUIST, B., OSHER, S. AND CHAKRAVARTHY, S. 1987 Uniformly High-Order Accurate Essentially Nonoscillatory Schemes, III. J. of Computational Physics, 71, pp.231-303

HINO, T. 1994 A Study of Grid Dependence in Navier-Stokes Solutions for Free Surface Flows around a Ship Hull. J. of The Society of Naval Architecs of Japan, 71

HINO, T. 2000 Unstructured Grid Flow Solver for Practical Ship Hulls. Gothenburg 2000 a Workshop on Numerical Ship Hydrodynamics

HOCHBAUM, A.C. AND SCHUMANN, C. 1999 Free Surface Viscous Flow around Ship Models. 7th Int. Conf. Numerical Ship Hydrodynamics, Nantes, France, pp. 2.3-1~2.3-12

HOCHBAUM, A.C. AND VOGT, M. 2000 Flow and Resistance Prediction for a Container Ship. Gothenburg 2000 a Workshop on Numerical Ship Hydrodynamics

KIM, D.H. 2000 A Study on Numerical Methods for Nonlinear Wave-Making Problems. Ph.D. Dissertation, Department of Naval Architecture and Ocean Engineering in Seoul National University, Korea

KIM, H.T. AND KIM, J.J. 2001 Simulation of Turbulent Flow and Surface Wave Fields around Series-60 C_B=0.6 Ship Model. J. of Ship & Ocean Technology, 5, No. 1, pp. 38-54

KIM, W.J., KIM, D.H., AND VAN, S.H. 1999 Calculation of Turbulent Flows around VLCC Hull Forms with Stern Frameline Modification. 7th Int. Conf. Numerical Ship Hydrodynamics, Nantes, France pp. 3.4-1~3.4-13

LAUNDER, B.E. AND SPALDING, D.B. 1974 The Numerical Computation of Turbulent Flows. Comp. Meth. Appl. Mech. Eng., 3, pp. 269-289

LEE S.H. 1997 Three-Dimensional Incompressible Viscous Solutions based on The Physical Curvilinear Coordinate System. Ph.D. Dissertation, Department of Computational Engineering in the College of Engineering, Mississipi State, Mississipi

MUZAFERIJA, S. 1994 Adaptive Finite Volume Method for Flow Predictions Using Unstructured Meshes and Multigrid Approach. Ph.D. Dissertation, University of London

PARK, I.R. 2000 Applications of a Level-set Method to Incompressible Viscous Flow with the Free Surface. Ph.D. Dissertation, Department of Naval Architecture and Ocean Engineering in Pusan National University, Korea

PARK, I.R. AND CHUN H.H. 1999(a) Analysis of Flow around a Rigid Body in Water-Entry & Exit Problems. J. of the Society of Naval Architects of Korea, 36, No. 4, pp. 37-47

PARK, I.R. AND CHUN H.H. 1999(b) A Study on the Level-Set Scheme for the Analysis of the Free Surface Flow by a Finite Volume Method. J. of the Society of Naval Architects of Korea, 36, No. 2, pp. 40-49

PENG, D.P., OSHER, S., ZHAO, H.K. AND KANG M.G. 1999 A PDE-Based Fast Local Level Set Method. J. of Computational Physics 155, pp. 410-438

STONE, H.L. 1968 Iterative Solution of Implicit Approximations of Multidimensional Partial Differential Equations. SIAM J. Numer. Anal., 5, pp. 530-558

SUSSMAN, M., FATEMI, E., SMEREKA, P., AND OSHER, S. 1997 An Improved Level Set Method for Incompressible Two-Phase Flows. Computers and Fluids, 27, No.5-6, pp. 663-680

TAHARA, Y. AND STERN, F.   1996   A Large-Domain Approach for Calculating Ship Boundary Laryers and Wakes for Nonzero Froude Number. J. of Computational Physics, **127**, pp. 398-411

TODA, Y., STERN, F. AND LONGO, J.   1991   Mean-flow Measurements in the Boundary Layer and Wake and Wave Field of a Series-60 C_B=0.6 Ship Model for Froude Numbers 0.16 and 0.316. IIHR Report No. 352, Iowa Institute of Hydraulic Research, The Univ. of Iowa, Iowa City, Iowa

VAN DOORMAL, J.P. AND RATHBY, G.D.   1984   Enhancements of the SIMPLE Method for Predicting Incompressible Fluid Flows. Numer. Heat Transfer, **7**, pp. 147-163

VOGT, M.   1998   A Numerical Investigation of the Level-set Method for Computing Free Surface Waves. Department of Naval Architecture and Ocean Engineering, Chalmers University of Technology, Report CHA/NAV/R-98/0054